2.2 Standard Model Processes and Simulations

We begin by describing the basic assumptions underlying our study of the physics capabilities of the NLC. We will briefly discuss the expected energy and luminosity that the NLC will provide, the performance of the detector that we expect to have available, our simulation methods, and the magnitudes of the most important standard model background processes.

2.2.1 Accelerator and Detector

The NLC is envisaged as the first full-scale e^+e^- linear collider, a machine designed from the beginning with the goal of high-luminosity colliding beam physics and one which takes account of the lessons of its prototype, the SLC. The NLC will be designed for an initial energy of 500 GeV in the center of mass, with an upgrade path to 1.5 TeV. It will provide a luminosity sufficient for a thorough experimental program on e^+e^- annihilation to standard and exotic particle pairs. It will provide a highly polarized e^- beam, and possibly also a polarized positron beam. Our basic assumptions on luminosity as a function of energy and on polarization are given in Table 2.1. These assumptions are justified in the description of the accelerator design given in Chapter 3 of this report and, at greater length, in [1].

Table 2.1: Basic Parameters of the Next Linear Collider

Energy (GeV)		Luminosity (cm^{-2}s^{-1})	
	500 GeV	5×10^{33}	
	1000 GeV	1×10^{34}	
	1500 GeV	1×10^{34}	
Polarization:			
		80% e^-, 0% e^+	Initial
		90% e^- 65% e^+	Possible

The NLC experiments can be carried out with a standard 4π multipurpose detector similar to those at LEP or SLC. In our concept of this detector, we include some innovations such as all-silicon tracking to minimize the effect of machine-related backgrounds, but for the most part the demands we have made on the detector are straightforwardly met. The essential performance assumptions we have made are shown in Table 2.2. Because of the small beam spot sizes at a linear collider, which allows us to bring a CCD vertex detector within 2 cm of the interaction point, the detector should have excellent b-tagging capabilities. The assumed curve of efficiency versus purity for b-tagging is shown in Fig. 2.1; the performance required has already been demonstrated in the SLD vertex detector.

Table 2.2: Summary of the detector parametrization used in the simulations. Smeared quantities are denoted in the table by a subscript s.

Particle	Energy	Momentum
Electrons	$\frac{\delta E}{E} = \frac{12\%}{\sqrt{E}} + 1.0\%$ $E_s = E + \delta E$	$P_s^2 = E_s^2 - m_e^2$
Photons	$\frac{\delta E}{E} = \frac{12\%}{\sqrt{E}} + 1.0\%$ $E_s = E + \delta E$	$P_s = E_s$
Neutral Hadrons	$\frac{\delta E}{E} = \frac{45\%}{\sqrt{E}} + 2.0\%$ $E_s = E + \delta E$	$P_s^2 = E_s^2 - m_\pi^2$
Charged Hadrons	$E_s^2 = P_s^2 + m_\pi^2$	$\frac{\delta P_{x,y}}{P_{x,y}^2} = 0.0005 \oplus \frac{0.0015}{P_{x,y}\sqrt{P}(\sin\theta)^{2.5}}$ $\frac{\delta P_z}{P_z^2} = \frac{0.0015}{P_{x,y}\sqrt{P}(\sin\theta)^{2.5}}$ $(P_s)_i = P_i + \delta P_i$

2.2.2 Simulations

In the studies presented here, the detector model has been used in concert with a set of familiar and newly-written simulation programs. In general, the background processes were generated by PYTHIA 5.7 [2], except for the background from $e^+e^- \to W^+W^-$, which plays an especially important role at linear collider energies. For this process we used a new generator [3] which is based on the formalism for this reaction presented by Hagiwara *et al.* [4]. This generator computed the total amplitude for W^+W^- production and subsequent decay to four fermions, retaining the full spin correlations through the process. It did make the approximation of treating the W's as on-shell particles, but it properly treated the effects of initial state electron polarization, beamstrahlung, collinear multi-photon initial state bremsstrahlung, and a nonzero W boson decay width. The same Monte Carlo program was used in the studies of nonstandard W physics reported in Sections 6 and 7. Many of the other analyses used specialized generators at this level of sophistication to simulate the new physics processes. These are described in the various sections of this report. Except where it is reported otherwise, the hadronization of partons and subsequent decays were performed by JETSET 7.4 [2].

Four-vectors of stable particles emerging from the simulated reaction were adjusted by a detector resolution smearing routine, which implemented the parametrization summarized in Table 2.2. All quantities were parametrized as a function of theta. The smearing assumed Gaussian errors and populated tails out to 3.5σ. The parametrization assumed a dead cone about the beampipe of 150 mrad ($\cos\theta = 0.99$). The neutral particle and charged

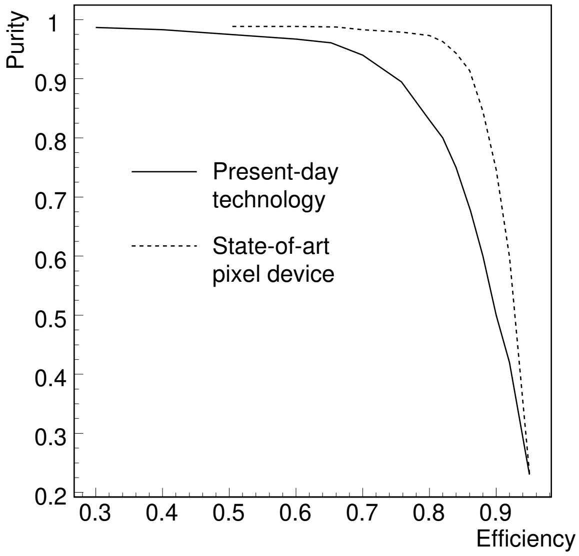

Figure 2.1: Efficiency versus purity relation for b-tagging with the NLC detector.

particle detection efficiencies were each taken to be 98%. For neutral hadrons, the momentum directions were Gaussian smeared in a cone about the original direction with a half-width of 15 mrad to simulate finite directional resolution. For photons and electrons, the directions were smeared by a cone of half-width 10 mrad.

2.2.3 Standard Model Processes at the NLC

Standard model processes, in addition to being interesting in their own right, are the background to searches for new physics at the NLC. Many of the standard model reactions at the NLC are familiar at lower energies and need only be extrapolated to higher energies. However, new processes, such as the pair production of gauge bosons, emerge as dominant reactions.

The cross sections of Standard Model processes at an e^+e^- collider are shown as a function of center of mass energy in Fig. 2.2 [5]. From left to right across this plot, the familiar e^+e^- annihilation processes fall with energy according to the point cross section for $e^+e^- \to \mu^+\mu^-$ in QED,

$$1 \text{ R} = \frac{4\pi\alpha^2}{3s} = \frac{87 \text{ fb}}{s \text{ (TeV}^2)} \ . \tag{2.2}$$

At the same time, new processes involving pair production and multiple production of weak interaction vector bosons become important.

Another view of the standard model backgrounds is given in Fig. 2.3, where the cross sections for the dominant e^+e^- annihilation processes are shown as a function of the degree of longitudinal polarization. The curves were calculated using ISAJET 7.13 [6]. The peripheral

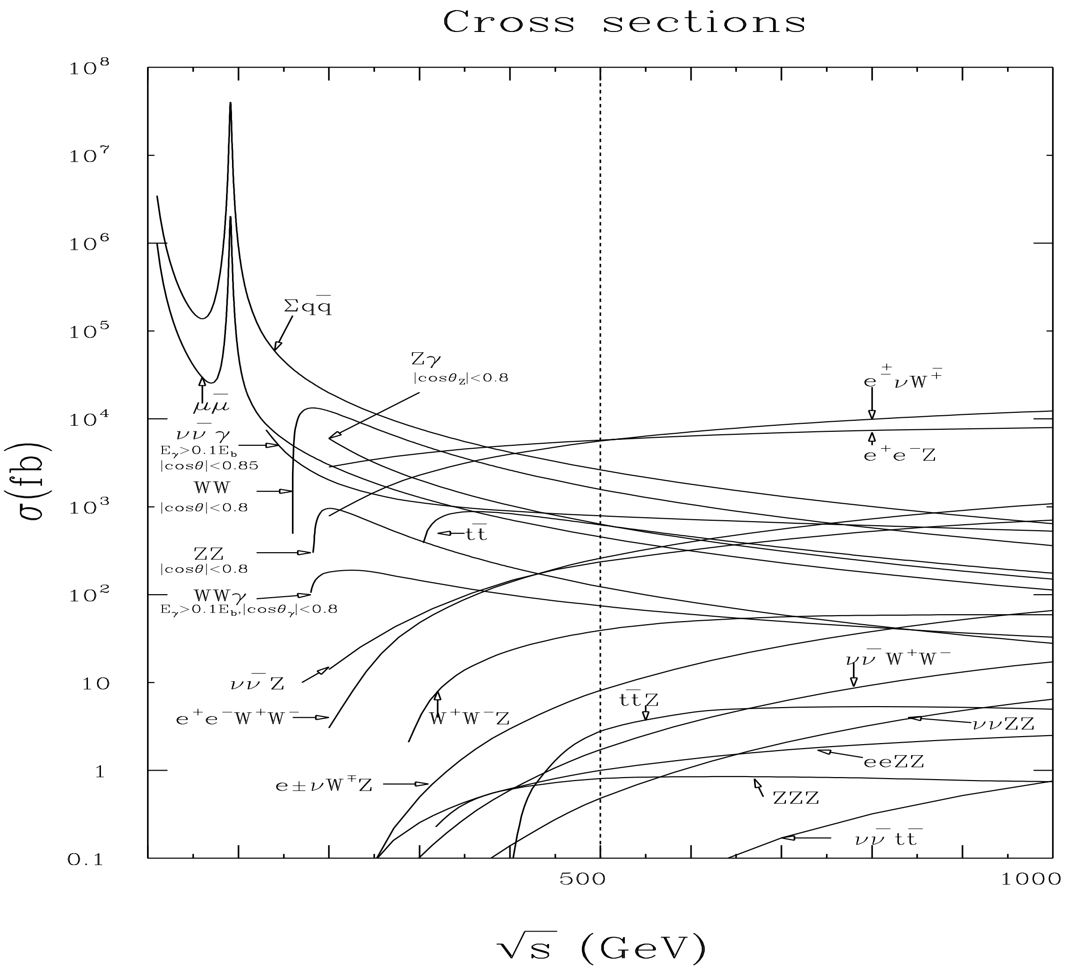

Figure 2.2: Cross sections for Standard Model physics processes in e^+e^- annihilation, as a function of center of mass energy, from [5].

two photon, t-channel Bhabha scattering and $e^+e^- \to Z^\circ\gamma$ processes are not shown; the cross sections for these reactions are relatively independent of polarization. The reactions $e^+e^- \to e^+\nu W^-, e^-\overline{\nu}W^+, e^+e^-Z^0$ are also not shown. The first of these is present only for left-handed e^-; the other two depend only weakly on e^- beam polarization. The most troublesome source of background in many of the physics analyses is the reaction $e^+e^- \to W^+W^-$, whose special role we have already pointed out. It is noteworthy that the cross section for this process can be reduced substantially by adjusting the electron beam polarization.

Cuts on other quantities, such as the acoplanarity and production angle will also be useful for removing standard model background. The distributions in these variables for standard model annihilation processes are shown in Figs. 2.4 and 2.5.

In general, the two photon and $e^+e^- \to Z^0\gamma$ processes are not important as backgrounds to annihilation processes because they may be removed easily from the data sample by low transverse momentum and multiplicity cuts [7]. The cross section for Bhabha scattering is

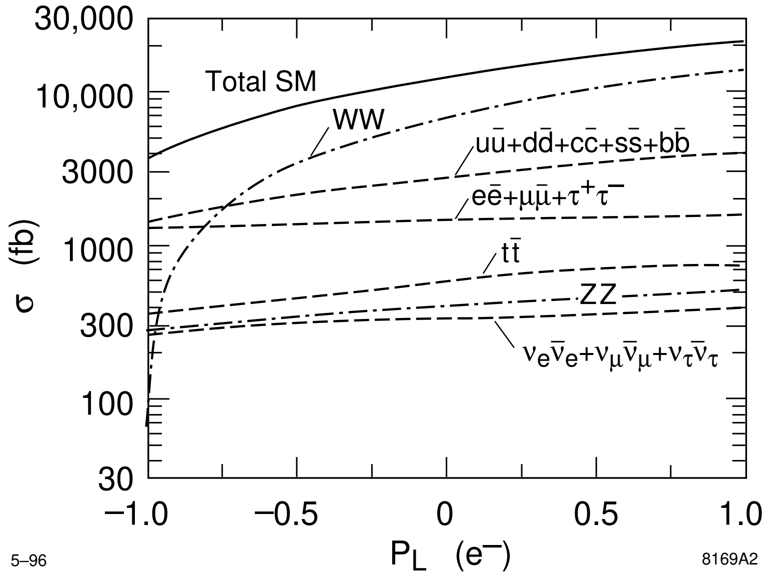

Figure 2.3: Cross sections for Standard Model physics processes in e^+e^- annihilation at 500 GeV, as a function of the electron longitudinal polarization.

very large in the forward direction but drops to a few units of R at large angles.

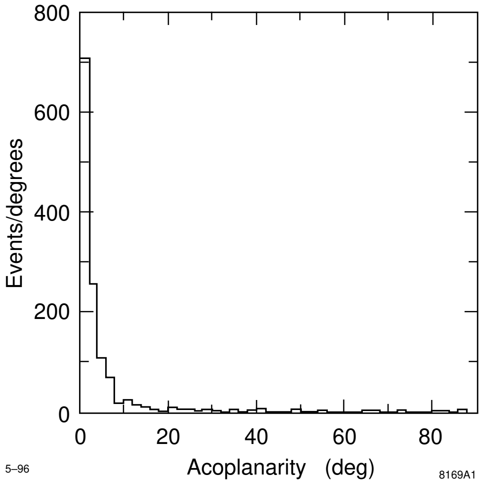

Figure 2.4: Expectation for the acoplanarity distribution in $e^+e^- \rightarrow W^+W^-$ events in which both W bosons decay to hadrons.

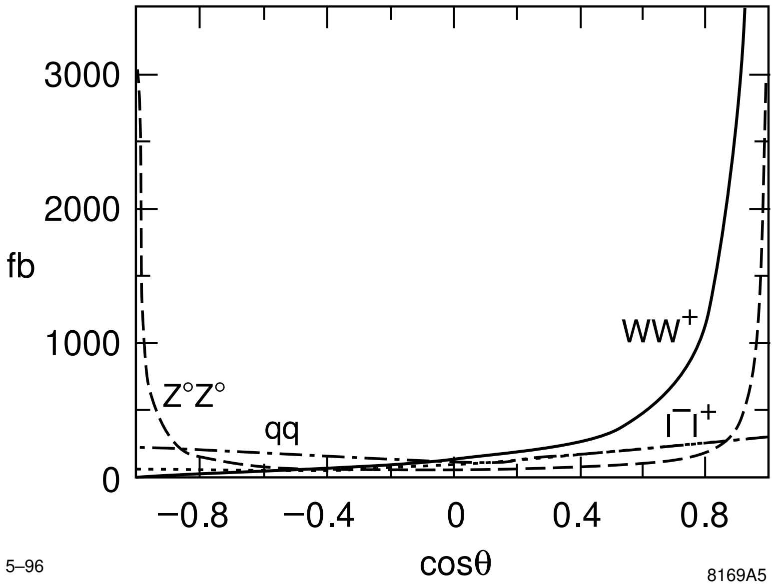

Figure 2.5: Expectation for the $\cos\theta$ distribution due to standard model processes.